

4.1 SUBFILTER SCALE FLUXES IN THE MARINE SURFACE LAYER: RESULTS FROM THE OCEAN HORIZONTAL ARRAY TURBULENCE STUDY (OHATS)

Peter P. Sullivan^{1*}, James B. Edson², Thomas W. Horst¹, John C. Wyngaard³ and Mark Kelly⁴

¹National Center for Atmospheric Research, Boulder, CO

²Department of Marine Sciences, University of Connecticut, Groton, CT

³Departments of Meteorology & Mechanical Engineering, Pennsylvania State University, State College, PA

⁴Department of Meteorology, Pennsylvania State University, State College, PA

1. INTRODUCTION

A goal of marine surface layer research is to identify and quantify coupling mechanisms that connect the atmospheric boundary layer and surface waves. Large-eddy simulation (LES) plays a role in this research and has provided insight into the interactions between imposed waves and turbulence (Sullivan et al., 2004, 2006). However, the fidelity of subfilter-scale (SFS) parameterizations used in LES for flows over complex geometry, *e.g.*, a moving surface gravity wave field, is untested. Recent field campaigns such as the Horizontal Array Turbulence Study (HATS) conducted over land have provided new impetus to improve parameterizations in LES codes (*e.g.*, see Sullivan et al., 2003; Kleissl et al., 2004; Chen and Tong, 2006; Hatlee and Wyngaard, 2006). A natural progression in these investigations is then to study increasingly complex flows. In the present work we present results from a new field campaign, the Ocean Horizontal Array Turbulence Study (OHATS), specifically directed at the measurement of SFS variables in the marine surface layer in the presence of surface waves. These observations can be used to examine and improve the SFS parameterization in LES codes, and more broadly, the impacts of water waves on surface layer turbulence under a variety of atmospheric stability conditions and wave states. Ultimately, the dataset and derived improvements to LES can benefit surface-layer parameterizations in mesoscale and numerical weather prediction models.

2. OHATS FIELD CAMPAIGN

The location for OHATS is the coastal region south of Martha's Vineyard openly exposed to the Atlantic Ocean. This site was selected as it has unique observational facilities to carry out marine field campaigns. One of the novel measuring platforms used in OHATS is a low-

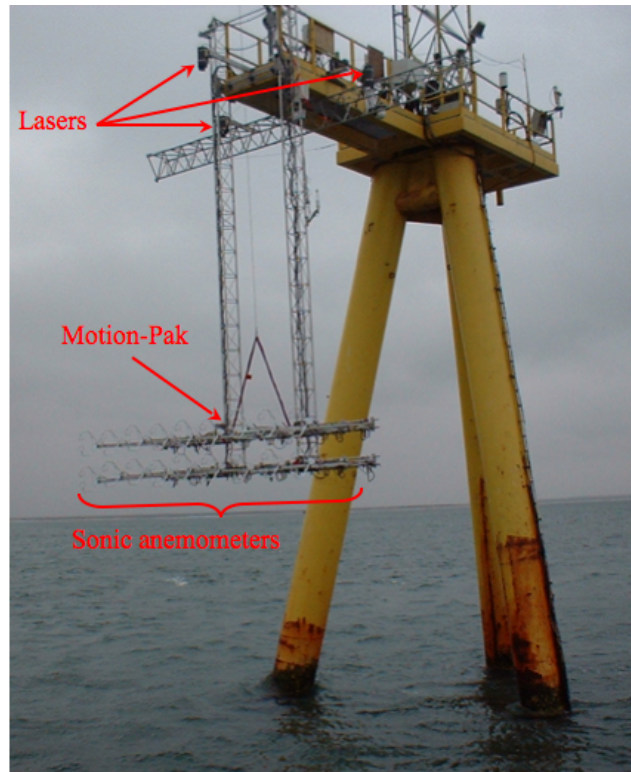


Figure 1: Photograph of the OHATS deployment showing the twin arrays of sonic anemometers, laser altimeters, Motion-Pak, and ASIT.

profile air-sea interaction tower (ASIT) located approximately 3.2 km off the coast in water 15m deep. Edson et al. (2006) provide further details about the Martha's Vineyard Coastal Observatory and the capabilities of the ASIT. The intensive observation period for OHATS extended from August to October 2004, approximately 85 days.

A photograph of the OHATS field site and sensor configuration is provided in Figure 1. A specially configured rack consisting of twin radio tower sections was designed and built to hold two horizontal booms from

*corresponding author address: Peter P. Sullivan, National Center for Atmospheric Research, P. O. Box 3000, Boulder, CO 80307-3000; email: pps@ncar.ucar.edu

which 18 CSAT3 sonic anemometers were mounted (9 sonics mounted on each horizontal boom). The physical restrictions imposed by the size of the ASIT diving board and the limited working space atop the platform placed constraints on the design of the anemometer rack. The vertical tower sections are 13m in length, with a horizontal separation of 1.3m, and are solidly attached to the ASIT diving board. The sonic carrying (horizontal) booms are approximately 4.6m in length. For OHATS, we settled on a configuration of two horizontal booms deployed at a nominal height of 5m and 5.5m above the sea surface with the horizontal spacing between sonics equal to 0.58m. The vertical placement of the sonic anemometers is chosen as a compromise between the desire to gather turbulence measurements close to the sea surface but also avoid swamping the rack except for very high sea states. The horizontal and vertical spacings in OHATS are comparable to the smallest configuration used in HATS¹. Preliminary tests at a land field site showed that sonic arrays with the OHATS spatial density do not induce significant flow distortion. The position of the rack is sufficiently upwind of the ASIT to avoid significant interference from the tower legs, about 7.5 leg diameters. For the wave measurements, 3 downward pointing Riegel laser altimeters are mounted in a triangular pattern to the catwalk attached directly beneath the ASIT diving board. The horizontal spacing of the altimeters is approximately 2 m and this configuration allows measurement of wave amplitude and propagation direction.

3. DATA ANALYSIS

Digital data from all instruments were first logged on the ASIT, then transmitted via cable links to the shore laboratory at Martha's Vineyard Coastal Observatory, and finally distributed through the Internet to NCAR. A complete archive of the field campaign, approximately 100 gigabytes of data, currently resides on the Mass Storage System at NCAR. To accommodate varied software applications and computational platforms the data is stored in standard netcdf (network common data form) files. A typical netcdf file contains 4 hours of data collected from 19 sonic anemometers (3 velocity components and virtual temperature), 3 laser altimeters (heights above the sea surface), and 3 accelerometers all sampled at a rate of 20hz. Running 5-minute averages of selected statistics for the duration of the field campaign can be viewed at <http://www.atd.ucar.edu/rtf/projects/OHATS04/qcdata/>.

¹HATS was conducted over a fallow field in California and used 4 different sonic setups. A description of the field site, data analysis procedures, and results are given by Horst et al. (2004); Sullivan et al. (2003).

A novel suite of software tools is used to process OHATS data. We improved and streamlined our existing codes that carry out spatial filtering of total velocity fields and compute various statistical measures of SFS variables. We added new routines to analyze the measured wave fields and to quantify the steadiness of the atmospheric conditions.

Computation of SFS variables requires that the atmospheric conditions be statistically stationary and at the same time have preferred wind directions; conditions with mean winds aligned within a ± 35 degree window normal to the array are considered optimum (Horst et al., 2004). Candidate time periods are first identified by visual inspection of the running 5-minute averages of wind direction, wind speed, and temperature over all days of the field campaign. This initial pass through the OHATS database identified about 275 hours for future detailed analysis, *i.e.*, approximately "12 days of data". This subset of the OHATS database covers a wide range of atmospheric stability conditions and wave states. At this stage, the database is split into 550 30-minute periods and quantitative checks for stationarity are then applied.

To facilitate rapid (and repetitive) processing of this large data volume a customized parallel processing code was developed using the Message Passing Interface (MPI). Using 8 CPUs on an IBM SP5, approximately 15 minutes of wallclock time are needed to fully analyze the velocity, temperature and wave data from 18 sonics and 3 laser altimeters for all 550 periods of interest. The analysis code performs all spatial filtering operations needed to compute subfilter scale variables, computes a collection of statistical measures, and performs quantitative checks for stationarity of the winds. Output from this MPI analysis code is a small database used in plotting final results. The procedure described above is flexible, allowing different types of analysis modules to be added and rapidly sweeps through a wide range of atmospheric conditions exposing trends in the data.

4. PRELIMINARY RESULTS

Here we describe first results for the variation of SFS momentum and scalar fluxes obtained from the OHATS dataset. These new findings are compared to similar measurements taken over a land surface.

4.1 Bulk Properties

We extracted 350 30-minute periods from the 275 hours in the OHATS database that simultaneously satisfy our stationarity and angular orientation criteria. The bulk atmospheric properties and wave states during these periods are presented in figures 2 and 3. A range of unstable, neutral, and slightly stable conditions $-1 < z/L < 0.2$

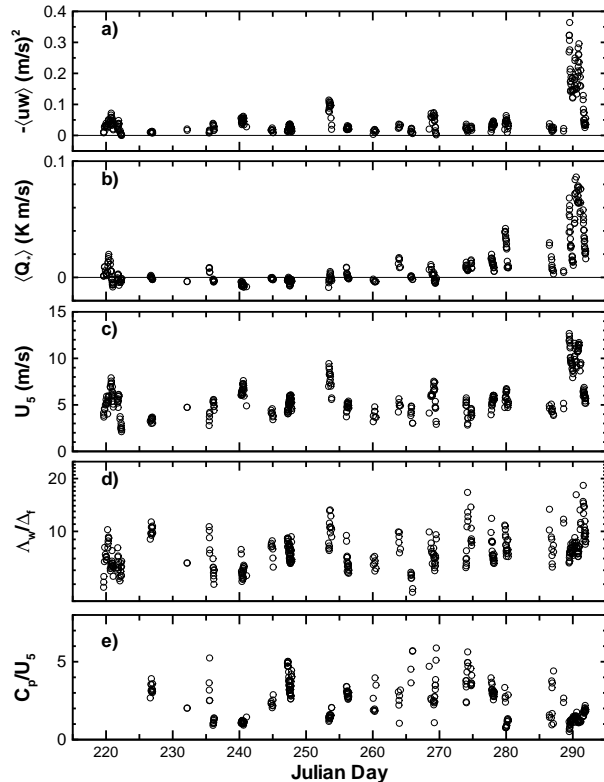


Figure 2: Variation of bulk atmospheric conditions and wave states during OHATS. a) vertical momentum flux, b) vertical heat flux, c) average mean speed at a nominal height $z = 5m$ above the sea surface, d) ratio of the peak scale in the vertical velocity spectrum to the horizontal filter width, and e) wave age.

are spanned with the majority of acceptable data obtained during near neutral conditions. The winds are generally light with the mean wind speed at $z = 5m$, $U_5 \sim 5ms^{-1}$; note a persistent strong wind event $U_5 > 10ms^{-1}$ occurred during the last week of the observational period. Consistent with the generally light winds the vertical momentum flux (normalized by air density ρ) varies from $0 < -\langle uw \rangle < 0.4(m/s)^2$ and the virtual heat flux ranges from $-0.02 < Q_* < 0.1 K\text{-}ms^{-1}$.

The wave state is an important parameter in our analysis and we expect the atmospheric turbulence to vary depending on whether the waves are traveling slower, equal to, or faster than the mean winds (Smedman et al., 1999; Grachev and Fairall, 2001; Sullivan et al., 2006, 2004, 2000). Here, the dominant phase speed of the wave field C_p is simply estimated from the peak in the wave spectrum. Based on the results in figure 2, most often the wind-wave conditions during OHATS are in a non-equilibrium (swell) state as the wave age parameter $C_p/U_5 > 1.2$. In these swell dominated regimes the wave

field can induce upward momentum transfer, *i.e.*, a momentum flux from the ocean to the atmosphere. Our LES results (Sullivan et al., 2004) show that “wave driven winds” also depend on the relative orientation between winds and waves, atmospheric stability, and persistence of the swell.

Figure 3 shows the ratio of the wavelength of the peak in the vertical velocity spectrum Λ_w to the filter width Δ_f . Sullivan et al. (2003) find that Λ_w/Δ_f is a crucial parameter and contains the essential information about stratification, vertical distance above the surface and filter size for stratified flows over stationary rough surfaces. In OHATS, $\Lambda_w/\Delta_f \sim [5, 15]$ which is a smaller range than was obtained in HATS. The narrower range results from the use of a single array spacing, *i.e.*, the horizontal distance between sonics is fixed in OHATS. The variability in Λ_w/Δ_f primarily reflects changing atmospheric conditions; mean wind angle variations also cause small reductions in Δ_f . The variation of z/Λ_w with stability z/L in OHATS (see figure 3) is broadly similar to that obtained over a stationary rough surface. Closer inspection of the results does however hint at a steeper slope as the atmospheric conditions cross from unstable to stable conditions.

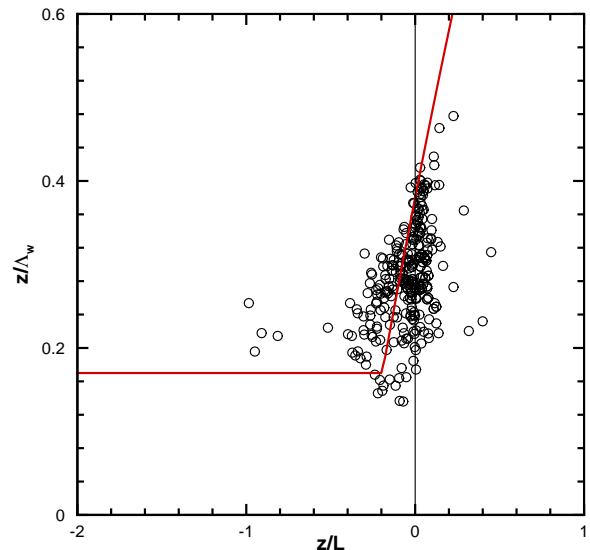


Figure 3: Variation of the peak scale in the vertical velocity spectrum versus the non-dimensional Monin-Obukhov distance z/L for OHATS. The solid red line is the result for flow over stationary roughness (from HATS, Sullivan et al. (2003)).

4.2 SFS Momentum Fluxes

SFS variables result from filtering the measured total fields of winds and virtual temperature (u_i, Θ) . The two-

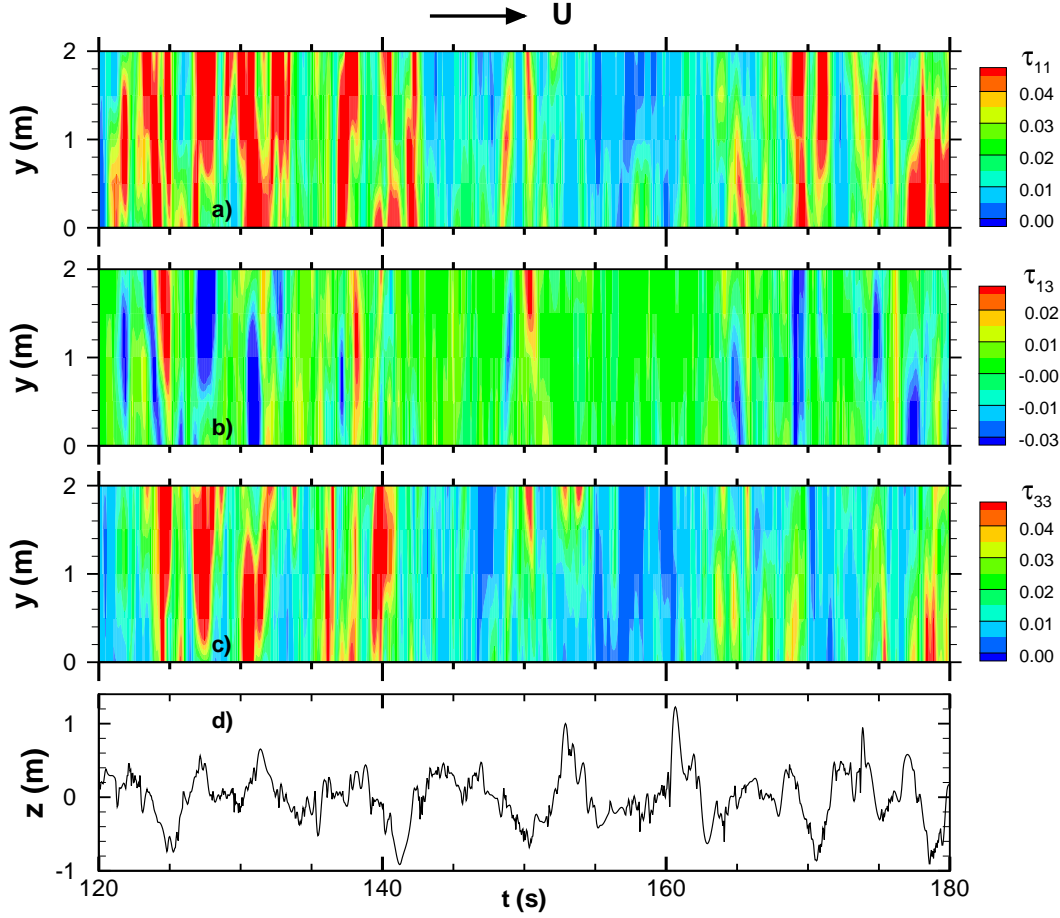


Figure 4: Typical time series of: a) SFS variance τ_{11} ; b) SFS flux τ_{13} ; c) SFS variance τ_{33} ; and d) wave height. Units of SFS fluxes are $(\text{m/s})^2$. Mean wind speed $\sim 4.64 \text{ ms}^{-1}$ and significant wave height $\sim 1.23 \text{ m}$.

dimensional filtering employed in OHATS is a combination of top-hat and Gaussian filters. Here the resolved (filtered) velocity is denoted \bar{u}_i and the SFS momentum fluxes are

$$\tau_{ij} = \overline{u_i u_j} - \bar{u}_i \bar{u}_j, \quad (1)$$

which are further decomposed into resolved-resolved interactions (a Leonard term L_{ij}), resolved-subfilter interactions (a cross term C_{ij}), and subfilter-subfilter interactions (a Reynolds term R_{ij}) using the Galilean invariant decomposition suggested by Germano (1986).

The stochastic nature of the SFS fluxes and wave field in OHATS is illustrated in figure 4. Notice the strong intermittent character of the fluxes at small scales in both space and time as the wave field evolves. Figures 5, 6, and 7 show average statistics of the SFS variables as functions of Λ_w/Δ_f . An important ingredient of most SFS modeling is the assumption of isotropy at the unresolved scales. In figure 5, we compare non-dimensional magnitudes of the (normal) SFS variances

$(\tau_{11}, \tau_{22}, \tau_{33})$. Here the SFS energy $E = \delta_{ij} \tau_{ij}/2$ and $3(\tau_{11}, \tau_{22}, \tau_{33})/2E = 1$ implies isotropic small scale motions. The trends are encouragingly similar to those in HATS. The variation of τ_{11} and τ_{33} however appear to be noticeably flatter as Λ_w/Δ_f increases. We might attribute this to the wave field but at the present time the exact cause of this variation is unknown. Notice that the SFS variances approach isotropy quite slowly as the filter width digs deeper into the inertial range. Even at $\Lambda_w/\Delta_f = 10$ the normalized SFS variances τ_{11} and τ_{33} are, respectively, $\sim 10\%$ larger and smaller than unity. Anisotropy is caused by the proximity of the lower boundary, wind shear, and wave field, effects not accounted for by Smagorinsky type SFS closures.

In figure 6 we decompose the SFS vertical momentum flux into its component parts, *i.e.*, $\tau_{13} = L_{13} + C_{13} + R_{13}$ and compare the variations to HATS. The most noticeable feature is the relative contributions of L_{13} and R_{13} to the SFS flux. Over waves the Leonard contri-

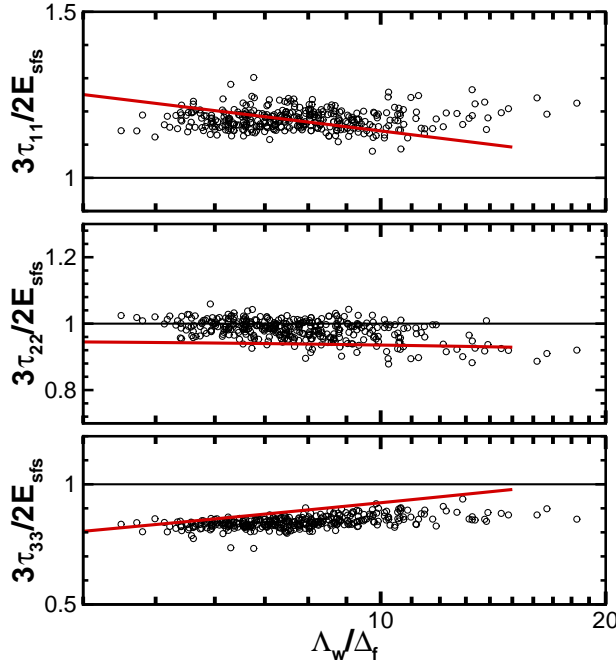


Figure 5: The isotropy of the SFS variances over ocean waves for varying atmospheric conditions. The deviation of the observations from the horizontal line in each figure is a measure of the anisotropy of the unresolved motions. The solid red line is a curve fit to the HATS results.

bution has increased substantially at the expense of the Reynolds term. L_{13} has a similar upward trend with increasing Λ_w/Δ_f as HATS, but is about a factor of two times larger over the entire range of Λ_w/Δ_f . At the same time, the ratio R_{13}/τ_{13} is much reduced over waves and shows a clear indication of being negative. Kang and Meneveau (2005) find that large scale coherent structures can alter the subfilter scale fluxes and strain alignment and perhaps the wave field in the marine surface layer is acting in a similar capacity.

One of the important attributes of a SFS closure is to exchange energy at the correct rate between resolved and unresolved fields. In the kinetic energy equation for SFS energy the primary production source is

$$\mathcal{P} = -\tau_{ij}S_{ij} \quad (2)$$

where τ_{ij} and S_{ij} are SFS fluxes and resolved scale strains, respectively. Twin arrays of horizontal sonics allows us to compute a time series of the production \mathcal{P} from the measured fields and thus we can examine the statistics of the energy transfer in detail. Figure 7 shows just the forwardscatter contribution to SFS energy transfer

$$\mathcal{P}_{\text{frwd}} = \frac{1}{2}(\mathcal{P} + |\mathcal{P}|). \quad (3)$$

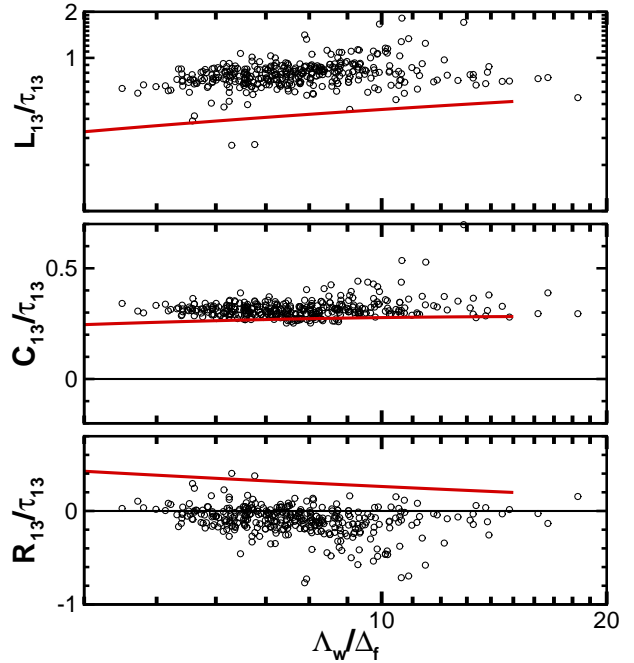


Figure 6: Decomposition of the subfilter scale vertical momentum flux into Leonard, cross, and Reynolds terms (L_{13}, C_{13}, R_{13}). The OHATS data has a greater contribution from the Leonard term compared to atmospheric flow over stationary roughness (note the logarithmic vertical scale in the upper panel). The red line is the result from HATS.

On average the *net* transfer is from the resolved field to the SFS motions, but instantaneously a small fraction of energy backscatter, *i.e.*, energy transfer from SFS to resolved motions, also occurs. With our normalization one can infer the backscatter contribution as $\mathcal{P}_{\text{back}} = 1.0 - \mathcal{P}_{\text{frwd}}$. Notice that over ocean waves the forwardscatter of energy does not exhibit the same upward trend with increasing Λ_w/Δ_f as does flow over stationary roughness. The results shown in Figures 6 and 7 hint that the wave field modifies the SFS fluxes and energy production in potentially important ways compared to flow over stationary roughness.

4.3 SFS Scalar Fluxes

Recently Wyngaard (2004a,b) proposed a new class of subfilter-scale models that are intended to be applicable across a range of scales spanning the gap $l \sim \Delta_f$ between the “LES limit” $l/\Delta_f \gg 1$ and the “mesoscale limit” $l/\Delta_f \ll 1$ with l the scale of the dominant turbulence². The mathematical steps outlining the methodology are

²In the present analysis Λ_w/Δ_f can be interpreted as a surrogate for l/Δ_f .

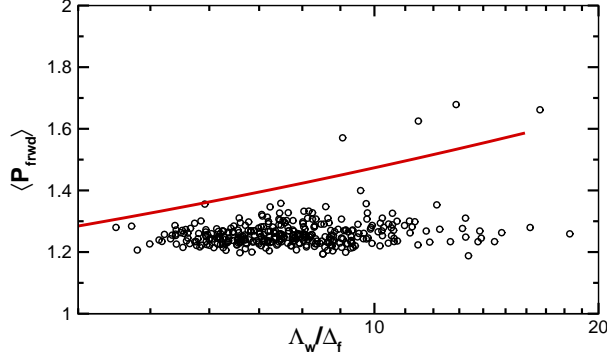


Figure 7: Forwardscatter of energy from the resolved field to the SFS field. $\langle P_{fwd} \rangle$ is normalized by the (net) mean energy transfer. The red line is the result from HATS.

fully described by Wyngaard (2004b). The basis of these simplified rate-equation models is rational truncation of the full transport equations for SFS fluxes based on scale analysis. These SFS prescriptions offer improvements to simple eddy viscosity closures, but have not yet been fully implemented and evaluated in simulation codes. Using a subset of the HATS database Hatlee and Wyngaard (2006) tested variants of these SFS closures for scalar and momentum fluxes. One of the important results from their investigation is the proper prediction of all components of SFS scalar flux. For a conserved scalar c the components of the SFS scalar flux

$$f_i = \overline{u_i c} - \overline{u_i} \overline{c}, \quad (4)$$

are modeled using a rate equation of the form

$$\frac{\partial f_i}{\partial t} = -f_j \frac{\partial \overline{u_i}}{\partial x_j} - \tau_{ij} \frac{\partial \overline{c}}{\partial x_j} - \frac{f_i}{T}. \quad (5)$$

This truncated model includes only time change, tilting and production terms and models pressure destruction via a sink of the form $-f_i/T$ with the time scale of the SFS turbulence

$$T = C \Delta_f / E^{1/2}. \quad (6)$$

In (6) $C \approx 0.3$ is a modeling constant chosen to match the HATS data (Hatlee and Wyngaard, 2006).

Algebraic stress models with some structural similarity to (5) have been proposed for stratified flows (*e.g.*, Findikakis and Street, 1979) and implemented in Reynolds-averaged Navier-Stokes (RANS) codes (*e.g.*, Hanjalic and Kenjeres, 2001), but only until recently have these types of models been validated against geophysical data in the context of LES. Here we test the applicability of (5) and (6) for scalar transport in turbulent flow over water waves.

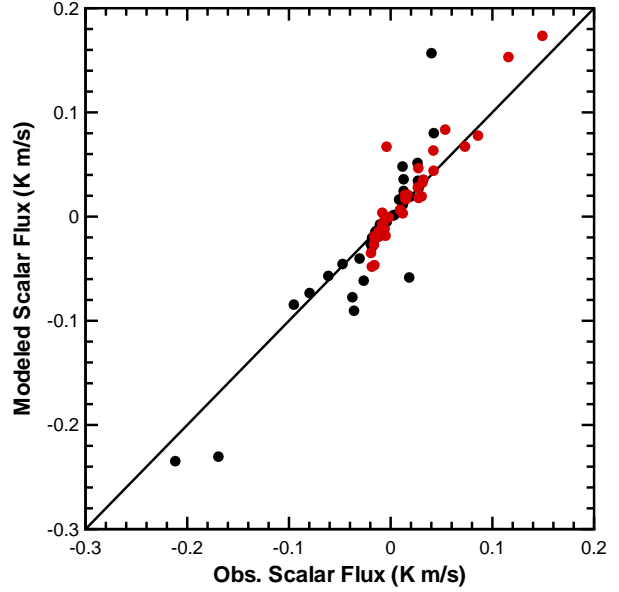


Figure 8: Comparison of modeled and observed SFS scalar flux in the atmospheric surface layer over a stationary rough surface. $\langle f_1 \rangle$ and $\langle f_3 \rangle$ are indicated by black and red dots respectively. The constant $C = 0.3$.

The OHATS database possesses all the ingredients necessary to evaluate the SFS closure given by (5) using virtual temperature θ as the conserved scalar c . Our algorithm advances (5) in time with a second-order Adams-Bashforth method. The observed values of SFS momentum fluxes and energy, resolved velocity and scalar gradients, which appear on the right-hand-side, are spline interpolated to increase their temporal resolution and thereby eliminate errors due to finite differencing. We performed an independent test of our algorithm using all the acceptable cases in the HATS database. Figure 8 shows the observed and modeled components of average scalar flux $\langle f_1 \rangle, \langle f_3 \rangle$; these results are in agreement with Hatlee and Wyngaard (2006) and verify the correctness of our algorithm. The findings illustrate that (5) is a good predictor for SFS scalar flux over a range of stratifications and filter widths over land. An important attribute of (5) is the prediction of a finite average value of horizontal scalar flux $\langle f_1 \rangle$; an eddy-viscosity scalar-gradient closure leads to $\langle f_1 \rangle = 0$ (Hatlee and Wyngaard, 2006).

Similar results for OHATS are depicted in figure 9. Inspection of the results shows that the prediction of horizontal scalar flux over waves is slightly below but closely follows the trend from HATS. However, (5) noticeably over predicts the SFS vertical scalar flux f_3 especially in cases with larger waves and scalar surface flux. Cases with significant wave heights greater than 1 m and at the same time surface convection exhibit the greatest separ-

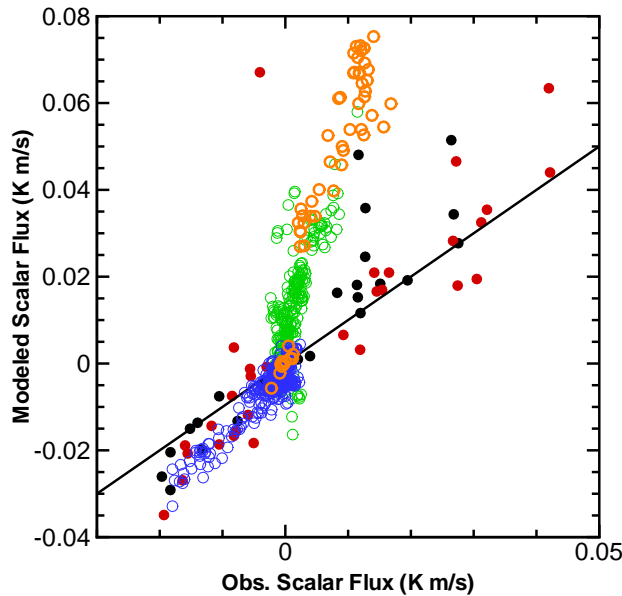


Figure 9: Comparison of modeled and observed SFS scalar flux in the marine surface layer over moving waves. Horizontal scalar flux $\langle f_1 \rangle$ is indicated by open blue circles. Vertical scalar flux $\langle f_3 \rangle$ is indicated by open green and orange circles; cases with significant wave height greater than 1 m are shown in orange. The results from HATS are the black and red dots. Note the difference in vertical and horizontal scales compared to figure 8. The constant $C = 0.3$.

ture from the HATS observations and predictions given by (5). The trends in figure 9 seem clear and hence the surprising result for f_3 merits further interrogation. Our first suspicion is that the wave field is inducing motions that are not accounted for in the modeling of the pressure destruction term and in particular the phase relationship between the wave induced pressure and scalar fields. In order to explore this speculation we need to identify the wave correlated motions in the velocity, pressure, and scalar fields. The direct numerical simulation (DNS) results for stratified flow over waves described by Sullivan and McWilliams (2002) will be further analyzed to gain insight into the present results.

5. SUMMARY

We have presented results from a new field campaign, the Ocean Horizontal Array Turbulence Study (OHATS), designed to obtain measurements of subfilter-scale variables in the marine surface layer. A first look at the data shows both similarities and differences with a comparable experiment carried out over a rough land surface (the Horizontal Array Turbulence Study). For example,

the results for the vertical component of SFS scalar flux show a clear wave signature while the variation of the normal components of the SFS momentum flux τ_{ij} are similar over land and water. The bulk of the OHATS observations are obtained under low wind conditions in the presence of fast moving swell, and thus the interactions between atmospheric turbulence and the wave field needs to be considered. The impact of swell and more generally the underlying wave field on SFS variables and their modeling are topics for future investigation. We plan to split the wind fields into turbulent and wavy contributions using the algorithm described by Hristov et al. (1998) in order to identify their separate contributions to the SFS fluxes and energy transfer.

Acknowledgments: We thank Tihomir Hristov and Edward Patton for useful discussions. This work is supported by the Office of Naval Research and the National Science Foundation. NCAR is sponsored by the National Science Foundation.

REFERENCES

- Chen, Q. and C. Tong, 2006: Investigation of the subgrid-scale stress and its production rate in a convective atmospheric boundary layer using measurement data, *J. Fluid Mech.*, **547**, 65–104.
- Edson, J., T. Crawford, J. Crescenti, T. Farrar, J. French, N. Frew, G. Gerbi, C. Helmig, T. Hristov, D. Khelif, A. Jessup, H. Jonsson, M. Li, L. Mahrt, W. McGillis, A. Plueddmann, L. Shen, E. Skillingstad, T. Stanton, P. Sullivan, J. Sun, J. Trowbridge, D. Vickers, S. Wang, Q. Wang, R. Weller, J. Wilkin, D. Yue, and C. Zappa, 2006: The coupled boundary layers and air-sea transfer experiment in low winds (CBLAST-Low), *Bull. Amer. Meteorol. Soc.*, **submitted**.
- Findikakis, A. N. and R. L. Street, 1979: An algebraic model for subgrid-scale turbulence in stratified flows, *J. Atmos. Sci.*, **36**, 1934–1949.
- Germano, M., 1986: A proposal for a redefinition of the turbulent stresses in the filtered Navier-Stokes equations, *Phys. Fluids*, **29**, 2323–2324.
- Grachev, A. A. and C. W. Fairall, 2001: Upward momentum transfer in the marine boundary layer, *J. Phys. Oceanogr.*, **31**, 1698–1711.
- Hanjalic, K. and S. Kenjeres, 2001: VLES of flows driven by thermal buoyancy and magnetic field, in *Modern Simulation Strategies for Turbulent Flow*, edited by B. J. Geurts, pp. 223–246, R. T. Edwards.
- Hatlee, S. C. and J. C. Wyngaard, 2006: Subfilter-scale modeling in the Terra Incognita, *J. Atmos. Sci.*, **submitted**.

- Horst, T. W., J. Kleissl, D. H. Lenschow, C. Meneveau, C.-H. Moeng, M. B. Parlange, P. P. Sullivan, and J. C. Weil, 2004: Field observations to obtain spatially-filtered turbulence fields from transverse arrays of sonic anemometers in the atmospheric surface layer, *J. Atmos. Sci.*, **61**, 1566–1581.
- Hristov, T., C. Friehe, and S. Miller, 1998: Wave-coherent fields in air flow over ocean waves: Identification of cooperative behavior buried in turbulence, *Physical Review Letters*, **81**, 5245–5248.
- Kang, H. S. and C. Meneveau, 2005: Effect of large-scale coherent structures on subgrid-scale stress and strain-rate eigenvector alignments in turbulent shear flow, *Phys. Fluids*, **17**, 1–20.
- Kleissl, J., M. Parlange, and C. Meneveau, 2004: Field experimental study of dynamic Smagorinsky models in the atmospheric surface layer, *J. Atmos. Sci.*, **61**, 2296–2307.
- Smedman, A., U. Högström, H. Bergström, and A. Rutgersson, 1999: A case study of air-sea interaction during swell conditions, *J. Geophys. Res.*, **104**, 25833–25851.
- Sullivan, P. P., J. B. Edson, T. Hristov, and J. C. McWilliams, 2006: Momentum flux structures and statistics in low-wind marine surface layers: Observations and large-eddy simulations, in *27th Amer. Meteorol. Soc. Symp. on Hurricanes and Tropical Meteorology*, Monterey, CA.
- Sullivan, P. P., J. B. Edson, J. C. McWilliams, and C.-H. Moeng, 2004: Large-eddy simulations and observations of wave driven boundary layers, in *16th Amer. Meteorol. Soc. Symp. on Boundary Layers and Turbulence*, Portland, ME.
- Sullivan, P. P., T. W. Horst, D. H. Lenschow, C.-H. Moeng, and J. C. Weil, 2003: Structure of subfilter-scale fluxes in the atmospheric surface layer with application to large-eddy simulation modeling, *J. Fluid Mech.*, **482**, 101–139.
- Sullivan, P. P. and J. C. McWilliams, 2002: Turbulent flow over water waves in the presence of stratification, *Phys. Fluids*, **14**, 1182–1195.
- Sullivan, P. P., J. C. McWilliams, and C.-H. Moeng, 2000: Simulation of turbulent flow over idealized water waves, *J. Fluid Mech.*, **404**, 47–85.
- Wyngaard, J. C., 2004a: Changing the face of small-scale meteorology, in *Atmospheric Turbulence and Mesoscale Meteorology*, edited by E. Federovich, R. Rotunno, and B. Stevens, pp. 17–34, Cambridge University Press.
- , 2004b: Toward numerical modeling in the Terra Incognita, *J. Atmos. Sci.*, **61**, 1816–1826.